Mendeleev Communications

Mendeleev Commun., 2026, **36**, 85–87

Sodium intercalation into the $NaNbTi(PO_4)_3$ NASICON-type phosphate

Ilia R. Cherkashchenko,[a,b] Rodion V. Panin,[b] Varvara A. Razuvaeva,[b] Alexey O. Polevik,[b] Daniil A. Novichkov,[b] Ivan V. Mikheev,[b] Evgeny V. Antipov[a,b] and Nellie R. Khasanova*[b]

[a] *Skolkovo Institute of Science and Technology, 143025 Moscow, Russian Federation*
[b] *Department of Chemistry, M. V. Lomonosov Moscow State University, 119991 Moscow, Russian Federation. E-mail: nelkh77@gmail.com*

DOI: 10.71267/mencom.7914

The $NaNbTi(PO_4)_3$ material with the NASICON structure (space group $R\bar{3}c$) was prepared by the Pechini-type technique followed by spark plasma sintering. XANES measurements revealed mixed-valence states of niobium ($Nb^{5+/4+}$) and titanium ($Ti^{4+/3+}$). The material exhibits reversible electrochemical intercalation of about 1.67 Na^+ per formula unit at a C/10 rate, with a gradual decrease in capacity, which could be attributed to the mixing of Na^+ and Ti^{3+} cations in the structure.

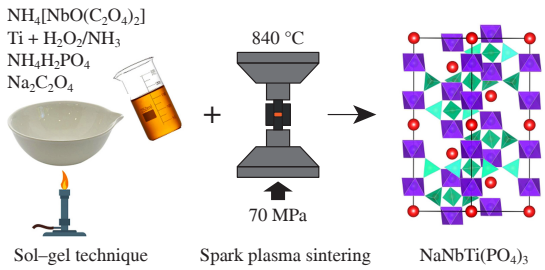

Keywords: NASICON-type materials, Pechini-type technique, spark plasma sintering, sodium insertion, reversible intercalation.

Global growth in energy consumption has created a pressing need for sustainable energy production and storage.[1–3] For the development of advanced electrochemical energy storage systems based on niobium redox processes, niobium oxides have been recognized as attractive materials with high chemical and thermal stability and high energy density.[4–6] The application of NASICON-type niobium phosphates as anode materials for Na-ion batteries enables full utilization of the reversible Nb^{5+}/Nb^{4+} (~2 V *vs.* Na^+/Na) and Nb^{4+}/Nb^{3+} (~1.1 V *vs.* Na^+/Na) transitions.[7,8]

Recently, we found that additional capacity can be achieved using mixed phosphates $NaNbM(PO_4)_3$ (M = V and Cr),[9,10] in which the M^{3+}/M^{2+} couple is active at low voltages (~1.5 V *vs.* Na^+/Na). This, combined with the $Nb^{5+}/Nb^{4+}/Nb^{3+}$ redox transitions, supports the $3e^-$ process per formula unit, resulting in a capacity of about 180 mAh g^{-1}. From this perspective, the introduction of titanium into $NaNbM(PO_4)_3$ appears to be the most advantageous choice due to its low cost, non-toxicity and the lowest M^{3+}/M^{2+} redox potential among NASICON-structured materials (~0.4 V *vs.* Na^+/Na).[11,12]

The previously reported NASICON-type phase $NaNbTi(PO_4)_3$ and its solid solutions $Na_xNbTi(PO_4)_3$ ($0 \leqslant x \leqslant 2$) have been prepared both by a high-temperature (~1000 °C) ceramic route from a multicomponent mixture of oxides and phosphates and *in situ* by sodiation of 'empty' $NbTi(PO_4)_3$ in a Na-half cell.[13–16] However, the electrochemical behavior of the stoichiometric $NaNbTi(PO_4)_3$ phase has not been investigated. In this article, we present a novel approach to the synthesis of $NaNbTi(PO_4)_3$ phosphate using a Pechini-type sol–gel method followed by spark plasma sintering (SPS) and report the electrochemical performance of the $NaNbTi(PO_4)_3$ material towards sodium intercalation.

The X-ray powder diffraction (XRPD) pattern of the obtained black sample was fully indexed in the rhombohedral unit cell[†] [Figure 1(*a*)]. No additional peaks were detected in the XPRD data, thus confirming the formation of amorphous carbon. This residual carbon arises from the thermal decomposition of organic components under argon atmosphere. According to thermogravimetric data (Figure S1, see Online Supplementary Materials), its amount was estimated to be 33–35 wt%. Elemental analysis of the $NaNbTi(PO_4)_3$ sample revealed the Na/Nb/Ti/P molar ratio of 1.03(5):1.02(5):1.07(5):3.0(1), confirming the stoichiometry of the phase. Rietveld refinement gave reliable structural parameters and interatomic distances characteristic of all elements (Tables S1 and S2, see Online Supplementary Materials). $NaNbTi(PO_4)_3$ crystallizes in a NASICON-type structure without any Ti/Nb ordering, and sodium ions occupy only the Na1 6*b* position, similar to the $NaNbM(PO_4)_3$ (M = Al, Cr, V) phases. Scanning electron microscopy (SEM) revealed that the sample consists of oblong micron-sized agglomerates combining submicron particles [Figure 1(*b*)].

The Nb *K*-edge XANES measurements (Figure 2) indicate that the spectrum of $NaNbTi(PO_4)_3$ is located between those of $TiNb^{V}(PO_4)_3$ and $Nb^{IV}O_2$, which serve as standards. Applying the linear combination analysis expansion technique, we determined the oxidation state of niobium to be +4.40(7), suggesting the coexistence of mixed-valent niobium ($Nb^{5+/4+}$) and titanium ($Ti^{4+/3+}$). This is consistent with previously published EPR and XANES data for $NaTiNb(PO_4)_3$[14] and $KTiNb(PO_4)_3$,[17] respectively.

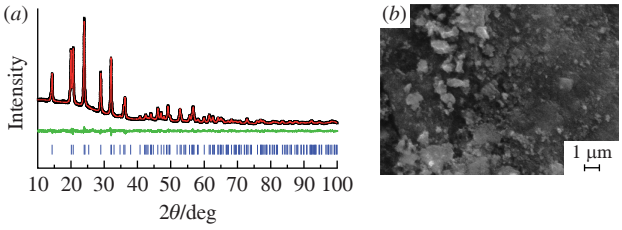

Figure 1 (*a*) XRPD pattern of the $NaNbTi(PO_4)_3$ phase and its Rietveld refinement with observed data points (black crosses), calculated pattern (red line), difference curve (green line) and Bragg positions (blue bars). (*b*) SEM image of the $NaNbTi(PO_4)_3$ sample.

[†] *Crystal data for* $NaNbTi(PO_4)_3$. Black powder, rhombohedral, space group $R\bar{3}c$, $a = 8.5867(1)$ and $c = 22.1346(4)$ Å, $V = 1413.35(3)$ Å^3, $Z = 6$. Rietveld refinement gave a satisfactory fit to the experimental XRPD profile ($R_I = 0.0127$, $R_p = 0.0175$, $R_{wp} = 0.0231$ and GOF = 2.76).

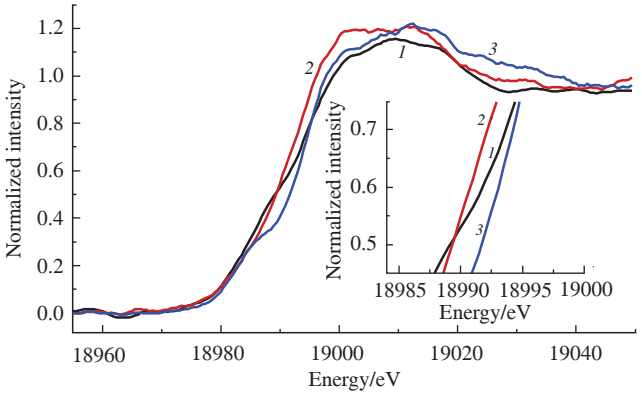

Figure 2 (*1*) Normalized Nb *K*-edge XANES spectrum of the pristine $NaNbTi(PO_4)_3$ compared with those of (*2*) NbO_2 and (*3*) $TiNb(PO_4)_3$ standards.

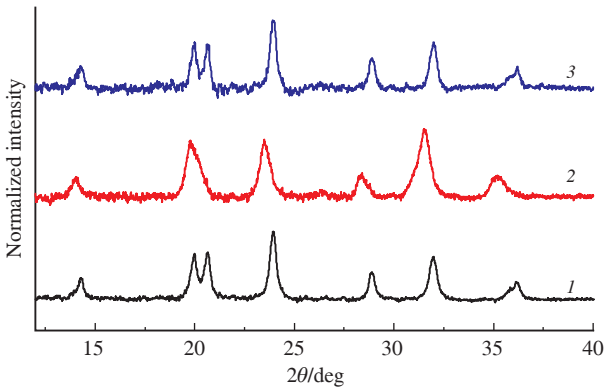

Figure 4 *Ex situ* XRPD patterns of the $NaNbTi(PO_4)_3$ electrodes: (*1*) initial, (*2*) charged to 0.8 V and (*3*) discharged to 3 V.

The cyclic voltammetry (CV) curves of $NaNbTi(PO_4)_3$ electrodes in the Na half-cell show two main pairs of peaks [Figure 3(*a*)]. The first one at ~2.1 V (*vs.* Na^+/Na) with a leftward shoulder is apparently related to the activity of both the Nb^{5+}/Nb^{4+} and Ti^{4+}/Ti^{3+} couples. The second peak is located at ~1.25 V (*vs.* Na^+/Na) and corresponds to the Nb^{4+}/Nb^{3+} redox transition. On the galvanostatic curves, [Figure 3(*b*)] two inclined regions were observed. The initial discharge capacity value is about 100 mAh g^{-1} (at a C/10 rate), which is lower than the theoretical value of 120 mAh g^{-1} calculated for the transfer of $2e^-$ per formula unit. Upon cycling, the discharge capacity continuously decreases, almost halving after the 10th cycle (Figure S2). The absence of any redox reactions at low potentials (down to 0.2 V *vs.* Na^+/Na) indicates that the Ti^{3+}/Ti^{2+} redox couple cannot be activated in this potential range (Figure S3).

Ex situ XRPD data (Figure 4) confirm the stability of the NASICON framework and the reversibility of $NaNbTi(PO_4)_3$ sodiation–desodiation processes. These data, combined with the results of electrochemical measurements, indicate a solid-solution mechanism of sodium intercalation into $NaNbTi(PO_4)_3$. It is worth mentioning a noticeable increase in the unit cell parameter *a*, associated with the extension of the $(Nb/Ti)O_6$ octahedron upon reduction of the *d*-metal (Table S3). The uptake of ~2 Na^+ into $NaNbTi(PO_4)_3$ results in a volume expansion of 6.1%, which agrees well with the value of ~9% for the case of insertion of 3 Na^+ ions (~3% per one Na^+ ion) in $NaNbM(PO_4)_3$ (M = Cr or V) materials.

The application of SPS for the synthesis of $NaNbM(PO_4)_3$ (M = Cr, Ti, V) phosphates appears to be a promising approach, as it reduces annealing time and prevents sodium loss during preparation, while maintaining phase stoichiometry. This is particularly important for $NaNbM(PO_4)_3$ (M = Ti and V) phosphates, which readily change oxidation state upon sodium loss. For vanadium, this problem can be circumvented using chemically bound sodium as the starting reagent (in the form of $NaVO_3$), which is not feasible when M = Ti. In this case, SPS ensures stoichiometry is maintained and prevents the formation of rutile-type impurities, most likely $(Nb,Ti)O_2$.

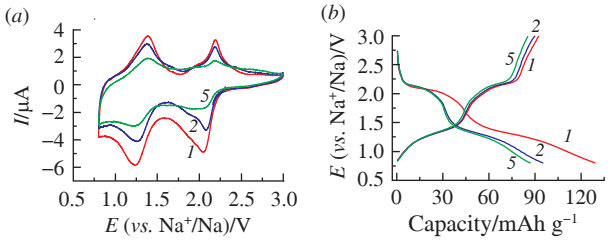

Figure 3 Electrochemical measurements of $NaNbTi(PO_4)_3$ in the potential range of 0.8–3.0 V (*vs.* Na^+/Na): (*a*) CV curves measured at 0.1 mV s^{-1} and (*b*) galvanostatic charge–discharge curves at a C/10 rate. Cycle numbers are indicated.

The obtained $NaNbTi(PO_4)_3$ phosphate shows electrochemical performance based on the $2e^-$ redox transition without the participation of the Ti^{3+}/Ti^{2+} redox couple, which contrasts with the behavior of $NaNbM(PO_4)_3$ (M = Cr, V) materials. Additionally, the cycling stability of $NaNbTi(PO_4)_3$ is lower than that of its V- and Cr-based analogs. This may be due to the migration of Ti^{3+} ions from octahedral to neighboring vacant trigonal-prismatic Na1 sites, similar to what has been observed for Mn^{2+} in the NASICON-type $Na_3MnTi(PO_4)_3$ phosphate.[18]

In the latter case, the process is reversible and can be prevented by deintercalation of two Na^+ ions, resulting in the formation of a Mn^{4+} ion, which is too small to occupy the Na1 site. In contrast, the migration of Ti^{3+} ions in $NaNbTi(PO_4)_3$ appears to be irreversible, since complete oxidation of titanium to Ti^{4+} requires the extraction of the last sodium atom from the NASICON structure, which is predominantly inactive.[19] Application of the $D_{M1(2)}$ criterion[20] for site selectivity, which is based on a comparison of the deviation degrees of ionic electronegativities and radii between the dopant and replaced elements, yields values of 0.76 for $M = Cr^{3+}$, 0.71 for $M = V^{3+}$ and only 0.56 for $M = Ti^{3+}$. The low value of the deviation degree for Ti^{3+} indicates a smaller disparity in its ability to occupy transition metal or sodium sites, resulting in Na^+/Ti^{3+} cation mixing. Moreover, these anti-site defects can accumulate cycle-by-cycle, blocking sodium pathways and reducing cycling stability. Therefore, we suppose that the electrochemical performance of $NaNbM(PO_4)_3$ phosphates, especially $NaNbTi(PO_4)_3$, may be affected by $M^{z+} \rightarrow Na^+(v)$ migration, similar to what has been observed in other NASICON-type materials such as $Na_3MnTi(PO_4)_3$,[21–23] $Na_3VCr(PO_4)_3$[24] and $Na_4MnCr(PO_4)_3$.[25]

The authors acknowledge the Russian Science Foundation (grant no. 23-13-00071) for support of this research. This work was also partially supported by the M. V. Lomonosov Moscow State University Program of Development (Labox-625 SPS machine). The authors are grateful to Dr. Dmitriy Stolbov for providing the SEM data and to Dr. Sergey Istomin for assistance with the TG experiments.

Online Supplementary Materials

Supplementary data associated with this article can be found in the online version at doi: 10.71267/mencom.7914.

References

1 Z. Xu and J. Wang, *Adv. Energy Mater.*, 2022, **12**, 2201692; https://doi.org/10.1002/aenm.202201692.

2 A. M. Skundin, T. L. Kulova and A. B. Yaroslavtsev, *Russ. J. Electrochem.*, 2018, **54**, 113; https://doi.org/10.1134/S1023193518020076.

3 A. Konarov, S.-T. Myung and Y.-K. Sun, *ACS Energy Lett.*, 2017, **2**, 703; https://doi.org/10.1021/acsenergylett.7b00130.
4 T.-F. Yi, H. Maleki Kheimeh Sari, X. Li, F. Wang, Y.-R. Zhu, J. Hu, J. Zhang and X. Li, *Nano Energy*, 2021, **85**, 105955; https://doi.org/10.1016/j.nanoen.2021.105955.
5 Q. Deng, Y. Fu, C. Zhu and Y. Yu, *Small*, 2019, **15**, 1804884; https://doi.org/10.1002/smll.201804884.
6 Y. Sheng, Y. Wang, S. Yin, L. Zhao, X. Zhang, D. Liu and G. Wen, *Chem. – Eur. J.*, 2024, **30**, e202302865; https://doi.org/10.1002/chem.202302865.
7 B. Patra, K. Kumar, D. Deb, S. Ghosh, G. S. Gautam and P. Senguttuvan, *J. Mater. Chem. A*, 2023, **11**, 8173; https://doi.org/10.1039/D2TA05971A.
8 I. R. Cherkashchenko, R. V. Panin, A. V. Babkin, D. A. Novichkov, E. V. Antipov and N. R. Khasanova, *Mendeleev Commun.*, 2025, **35**, 393; https://doi.org/10.71267/mencom.7637.
9 N. R. Khasanova, R. V. Panin, I. R. Cherkashchenko, M. V. Zakharkin, D. A. Novichkov and E. V. Antipov, *ACS Appl. Mater. Interfaces*, 2023, **15**, 30272; https://doi.org/10.1021/acsami.3c04576.
10 R. V. Panin, I. R. Cherkashchenko, V. V. Zaitseva, R. R. Samigullin, M. V. Zakharkin, D. A. Novichkov, A. V. Babkin, I. V. Mikheev, N. R. Khasanova and E. V. Antipov, *Chem. Mater.*, 2024, **36**, 6902; https://doi.org/10.1021/acs.chemmater.4c00933.
11 P. Senguttuvan, G. Rousse, M. E. Arroyo y de Dompablo, H. Vezin, J.-M. Tarascon and M. R. Palacín, *J. Am. Chem. Soc.*, 2013, **135**, 3897; https://doi.org/10.1021/ja311044t.
12 D. Wang, Q. Liu, C. Chen, M. Li, X. Meng, X. Bie, Y. Wei, Y. Huang, F. Du, C. Wang and G. Chen, *ACS Appl. Mater. Interfaces*, 2016, **8**, 2238; https://doi.org/10.1021/acsami.5b11003.
13 K. K. Rangan and J. Gopalakrishnan, *Inorg. Chem.*, 1995, **34**, 1969; https://doi.org/10.1021/ic00111a055.
14 L. Bennouna, S. Arsalane, R. Brochu, M. R. Lee, J. Chassaing and M. Quarton, *J. Solid State Chem.*, 1995, **114**, 224; https://doi.org/10.1006/jssc.1995.1032.
15 O. Tillement, J. C. Couturier, J. Angenault and M. Quarton, *Solid State Ionics*, 1991, **48**, 249; https://doi.org/10.1016/0167-2738(91)90039-E.
16 O. Tillement, J. Angenault, J. C. Couturier and M. Quarton, *Solid State Ionics*, 1992, **53–56**, 391; https://doi.org/10.1016/0167-2738(92)90405-E.
17 R. V. Panin, I. R. Cherkashchenko, D. A. Novichkov, I. V. Mikheev, D. N. Stolbov, E. V. Antipov and N. R. Khasanova, *Inorg. Chem. Commun.*, 2025, **172**, 113676; https://doi.org/10.1016/j.inoche.2024.113676.
18 J. Zhang, C. Lin, Q. Xia, C. Wang and X. S. Zhao, *ACS Energy Lett.*, 2021, **6**, 2081; https://doi.org/10.1021/acsenergylett.1c00426.
19 Z. Jian, C. Yuan, W. Han, X. Lu, L. Gu, X. Xi, Y.-S. Hu, H. Li, W. Chen, D. Chen, Y. Ikuhara and L. Chen, *Adv. Funct. Mater.*, 2014, **24**, 4265; https://doi.org/10.1002/adfm.201400173.
20 K. Li, J. Shao and D. Xue, *Funct. Mater. Lett.*, 2013, **6**, 1350043; https://doi.org/ 10.1142/S1793604713500434.
21 Y. Liu, X. Rong, R. Bai, R. Xiao, C. Xu, C. Zhang, J. Xu, W. Yin, Q. Zhang, X. Liang, Y. Lu, J. Zhao, L. Chen and Y.-S. Hu, *Nat. Energy*, 2023, **8**, 1088; https://doi.org/10.1038/s41560-023-01301-z.
22 C. Xu, W. Hua, Q. Zhang, Y. Liu, R. Dang, R. Xiao, J. Wang, Z. Chen, F. Ding, X. Guo, C. Yang, L. Yang, J. Zhao and Y.-S. Hu, *Adv. Funct. Mater.*, 2023, **33**, 2302810; https://doi.org/10.1002/adfm.202302810.
23 H. Zhang, Z.-Y. Gu, X.-T. Wang, X.-X. Zhao, Y.-L. Heng, Y. Liu, J.-L. Yang, S.-H. Zheng and X.-L. Wu, *Adv. Mater.*, 2024, **36**, 2410797; https://doi.org/10.1002/adma.202410797.
24 R. Liu, S. Zheng, Y. Yuan, P. Yu, Z. Liang, W. Zhao, R. Shahbazian-Yassar, J. Ding, J. Lu and Y. Yang, *Adv. Energy Mater.*, 2021, **11**, 2003256; https://doi.org/10.1002/aenm.202003256.
25 S. Chen, J. Hou, X. He, Q. Wang, W. Wang. M. Zhou, K. Wang and K. Jiang, *ACS Appl. Mater. Interfaces*, 2024, **16**, 52653–52662; https://doi.org/10.1021/acsami.4c10821.

Received: 10th September 2025; Com. 25/7914